Molecular Magnetic Resonance Imaging Accurately Measures the Antifibrotic Effect of EDP-305, a Novel Farnesoid X Receptor Agonist

Derek J. Erstad [iD],[1] Christian T. Farrar,[2] Sarani Ghoshal,[1] Ricard Masia,[3] Diego S. Ferreira,[2] Yin-Ching Iris Chen,[2] Ji-Kyung Choi,[2] Lan Wei,[1] Phillip A. Waghorn,[2] Nicholas J. Rotile,[2] Chuantao Tu,[2] Katherine A. Graham-O'Regan,[2] Mozhdeh Sojoodi,[1] Shen Li,[1] Yang Li,[4] Guogiang Wang,[4] Kathleen E. Corey,[5] Yat Sun Or,[4] Lijuan Jiang,[4] Kenneth K. Tanabe,[1] Peter Caravan,[2,6] and Bryan C. Fuchs[1]

We examined a novel farnesoid X receptor agonist, EDP-305, for its antifibrotic effect in bile duct ligation (BDL) and choline-deficient, L-amino acid-defined, high-fat diet (CDAHFD) models of hepatic injury. We used molecular magnetic resonance imaging with the type 1 collagen-binding probe EP-3533 and the oxidized collagen-specific probe gadolinium hydrazide to noninvasively measure treatment response. BDL rats (n = 8 for each group) were treated with either low or high doses of EDP-305 starting on day 4 after BDL and were imaged on day 18. CDAHFD mice (n = 8 for each group) were treated starting at 6 weeks after the diet and were imaged at 12 weeks. Liver tissue was subjected to pathologic and morphometric scoring of fibrosis, hydroxyproline quantitation, and determination of fibrogenic messenger RNA expression. High-dose EDP-305 (30 mg/kg) reduced liver fibrosis in both the BDL and CDAHFD models as measured by collagen proportional area, hydroxyproline analysis, and fibrogenic gene expression (all $P < 0.05$). Magnetic resonance signal intensity with both EP-3533 in the BDL model and gadolinium hydrazide in the CDAHFD model was reduced with EDP-305 30 mg/kg treatment ($P < 0.01$). Histologically, EDP-305 30 mg/kg halted fibrosis progression in the CDAHFD model. *Conclusion*: EDP-305 reduced fibrosis progression in rat BDL and mouse CDAHFD models. Molecular imaging of collagen and oxidized collagen is sensitive to changes in fibrosis and could be used to noninvasively measure treatment response in clinical trials. (*Hepatology Communications* 2018;2:821-835)

Farnesoid X receptor (FXR), a bile acid-responsive transcription factor, mediates multiple physiologic processes, including lipid metabolism, glucose homeostasis, and enterohepatic circulation of bile acids, and may be hepatoprotective for numerous gastrointestinal disorders, including cholestatic and fatty liver diseases.[1-3] An important pathogenic component of cholestatic liver disease involves toxic bile exposure to hepatocytes.[4,5] Injury to biliary epithelium results in local inflammation, loss of cholangiocyte tight junctions, and extravasation of bile salts, which induce local hepatocyte death and periductular fibrosis. Progressive cycles of inflammation, wound healing, and fibrosis lead to worsened cholestasis and eventually cirrhosis and hepatic failure.[6] FXR agonism might counteract the burden of cholestasis through down-regulation of bile acid production. FXR agonism may also be beneficial for fatty liver disease, which is driven by sublethal lipotoxic hepatocyte injury, resulting in a state of chronic inflammation, stellate cell activation, immune infiltration, and progressive fibrosis.[7] FXR stimulation has been shown to

reduce hepatic triglyceride production and regulate hepatocyte beta oxidation, potentially mitigating lipo-toxic injury.[8]

Nonalcoholic steatohepatitis (NASH), the active form of nonalcoholic fatty liver disease, and primary biliary cholangitis (PBC), an autoimmune cholestatic condition characterized by progressive injury to the biliary system, are two human conditions for which FXR agonists have been evaluated in clinical trials. In the United States, NASH affects 5% of the general population and up to 25% of patients who undergo bariatric surgery.[9,10] This disorder highly associates with obesity-related metabolic conditions, and up to 70% of cryptogenic cirrhosis diagnoses may be secondary to unmitigated NASH.[11,12] PBC is a rare disorder, with approximately 20-40 cases per 100,000 persons, and primarily affects women.[13,14] In 2016, the FXR agonist obeticholic acid (OCA), a semisynthetic derivative of chenodeoxycholic acid, was approved in the United States for treatment of PBC after meeting the primary endpoint of reduced alkaline phosphatase level in a phase III clinical trial. OCA is also currently being tested in a phase III clinical trial for treatment of NASH.

The U.S. Food and Drug Administration, however, recently announced a warning about increased risk of serious liver injury and death associated with OCA in patients with moderate to severe decreases in liver function.[15] Moreover, OCA treatment in humans is associated with significant elevation in low-density lipoprotein cholesterol and reduction of high-density lipoprotein cholesterol as well as increased pruritis. Therefore, there is an urgent need for newer therapies to treat PBC and NASH.

A historic limitation in the diagnosis and management of cholestatic and fatty liver disorders has been the lack of sensitive and specific noninvasive tests to monitor liver fibrosis.[16] Liver biopsy is the current gold standard, but it is invasive with inherent risks, particularly for patients with intrinsic liver disease who are at increased risk of bleeding and infection.[17] Molecular imaging of liver fibrosis holds great potential as a noninvasive method for diagnosing and monitoring progression of chronic liver disease. It has the following advantages: first, unlike biopsy, imaging captures the entire organ for a more accurate assessment of disease burden; second, liver imaging is noninvasive, thereby reducing risks and avoiding the need for post-procedural observation; third, due to greater safety and ease of use, molecular imaging provides a better alternative to monitoring response to therapy, particularly for future clinical trial design.

In this study, we test a novel small molecule, nonbile acid, selective FXR agonist, EDP-305, for its antifibrotic effect in two rodent models of cholestatic and fatty liver injury: bile duct ligation (BDL) in rats and

View this article online at wileyonlinelibrary.com.

ARTICLE INFORMATION:

From the [1]Division of Surgical Oncology, Massachusetts General Hospital, Harvard Medical School, Boston, MA; [2]Martinos Center for Biomedical Imaging, Massachusetts General Hospital, Harvard Medical School, Charlestown, MA; [3]Department of Pathology, Massachusetts General Hospital, Harvard Medical School, Boston, MA; [4]Enanta Pharmaceuticals, Watertown, MA; [5]Department of Medicine, Massachusetts General Hospital, Harvard Medical School, Boston, MA; [6]Institute for Innovation in Imaging, Massachusetts General Hospital, Boston, MA.

ADDRESS CORRESPONDENCE AND REPRINT REQUESTS TO:

Bryan C. Fuchs, Ph.D.
Division of Surgical Oncology, Massachusetts General Hospital
55 Fruit Street, WRN 401
Boston, MA 02114
E-mail: bfuchs@partners.org
Tel: +1-617-726-4174

choline-deficient, L-amino acid-defined, high-fat diet (CDAHFD) in mice. In addition, we noninvasively monitor liver fibrosis and fibrogenesis, our primary pathologic factors of interest, by employing two previously validated molecular magnetic resonance (MR) probes, EP-3533 and gadolinium hydrazide (Gd-Hyd), respectively.[18-22]

Materials and Methods

CELL CULTURE

Hepatic stellate cell (HSC) lines along with primary HSCs and hepatocytes, between passage 1 and 8, were seeded on uncoated plastic dishes.[23] Cells were treated with 10 μM concentration EDP-305 (dissolved in serum-free Dulbecco's modified Eagle's medium) and incubated for 72 hours. All cell culture experiments were performed in serum-free Dulbecco's modified Eagle's medium. Details regarding individual cell lines can be found in the Supporting Methods.

GENE EXPRESSION

Real-time quantitative polymerase chain reaction was performed on whole liver and ileum samples from treated and imaged animals.[24] Taqman primer sequences (Life Technologies, Carlsbad, CA) can be found in the Supporting Methods.

WESTERN BLOT

Primary antibodies used for this study included actin (#4970, 1:2,000 dilution; Cell Signaling, Beverly, MA), fibroblast growth factor receptor 4 (FGFR4) (ab119378, 1:1,000 dilution; Abcam, Cambridge, MA), and FXR (A9033A, 1:1,000 dilution; Thermo-Fisher, Waltham, MA).

ANIMAL MODELS

All experiments were performed in accordance with the National Institutes of Health's Guide for the Care of Use of Laboratory Animals and approved by the Institution's Animal Care and Use Committee. Male CD rats (n = 24) underwent BDL (Charles River Laboratories, Wilmington, MA). Control animals (n = 6) underwent a sham procedure. Male C57BL/6 mice (n = 24) were fed a CDAHFD consisting of 60% kcal fat and 0.1% methionine.[25] Control animals (n = 4) were fed normal chow. Drug treatment with EDP-305 was administered at either 10 mg/kg or 30 mg/kg doses by daily oral gavage. For the BDL model, drug treatments were started on day 4 after BDL and continued until days 17-18. For the CDAHFD model, drug treatments were started at the beginning of week 6 on the diet and were continued until week 12.

EP-3533

EP-3533 comprises a 10-amino acid cyclic peptide conjugated to three gadopentetate (Gd) moieties by a thiourea linkage. EP-3533 has a relaxivity of 48.3 mM^{-1}second^{-1} at 1.4T and binds specifically to type 1 collagen with Kd = 1.8 μM.[26,27]

Gd-Hyd

Gd-Hyd comprises a 1,4,7,10-tetraazacyclododecane-1,4,7,10-tetraacetate gadolinium chelate conjugated to a hydrazide moiety. Gd-Hyd has a relaxivity of 4.1 mM^{-1}second^{-1} at 1.4T and binds specifically to the allysine residues on oxidized collagen. Increased MR signal intensity on T1-weighted images is proportional to the degree of allysine present in tissue.[18]

MR IMAGING

Animals were anesthetized with 1%-2% isoflurane, with body temperature maintained at 37°C. For the BDL model, imaging was performed at 1.5T using a clinical MR imaging (MRI) scanner (Siemens Healthcare, Malvern, PA). Respiratory-gated, three-dimensional inversion, recovery images were acquired prior to and 60 minutes following intravenous administration of 10 μmol/kg EP-3533.[20] For the CDAHFD model, imaging was performed at 4.7T using a small bore animal scanner (Bruker, Billerica, MA). Baseline two-dimensional and three-dimensional fast low-angle shot (FLASH) images were acquired before and continuously for 30 minutes after injection of 100 μmol/kg Gd-Hyd. MR liver signal to noise ratio (SNR) was measured before and 25 minutes after Gd-Hyd injection, and the relative increase in SNR was computed (% ΔSNR).[28] A 2-point Dixon sequence was used to estimate liver fat content.[29] Imaging parameters can be found in the Supporting Methods.

PATHOLOGIC AND HISTOCHEMICAL ANALYSIS

The grade of steatosis was quantified as follows: grade 1, 5%-33%; grade 2, 33%-66%; grade 3, >66%).[30] Collagen proportional area (CPA) and

hepatic lipid vacuolization were calculated from whole-slide scanned sections using ImageJ (National Institutes of Health). Hydroxyproline was quantified by high-performance liquid chromatography analysis.[19-22]

SERUM LABORATORY ANALYSIS

A cardiac terminal blood withdrawal was performed at the time of sacrifice, and serum liver proteins, bilirubin, and lipids were measured (DRI-CHEM 4000 Chemistry Analyzer; Heska AG, Basel, Switzerland).[24,31]

STATISTICAL ANALYSIS

Results are expressed as mean $\pm$ 1 SD unless otherwise noted. One-way analysis of variance was followed by post-hoc Tukey tests with two-tailed distribution to analyze data among groups of three or more. The Student t test compared data between the control and one experimental group. $P < 0.05$ was considered significant.

Results

EDP-305 REDUCES SERUM MARKERS OF LIVER INJURY IN BDL RATS

EDP-305 treatment had no significant effect on body weight compared to BDL controls (Supporting Fig. S1A). Control BDL livers were significantly larger compared to sham (12 $\pm$ 0.6 g versus 19 $\pm$ 1.6 g; $P \leq$ 0.01). Neither FXR agonist significantly affected absolute liver weight compared to BDL control rats. Alanine aminotransferase was significantly reduced ($P \leq$ 0.01) in both low- (67 $\pm$ 7 U/L) and high-dose (62 $\pm$ 9 U/L) EDP-305 treatment groups compared to BDL control (146 $\pm$ 28 U/L) (Supporting Fig. S1B). Similarly, aspartate aminotransferase was significantly reduced ($P \leq$ 0.01) in both low- (260 $\pm$ 25 U/L) and high-dose (222 $\pm$ 20 U/L) EDP-305 treatment groups compared to BDL control (684 $\pm$ 80 U/L). Total bilirubin was significantly ($P \leq$ 0.01) increased in all BDL treatment groups compared to the sham group, consistent with the pathogenic mechanism of the model. There was no difference in serum triglyceride values among treatment groups.

EDP-305 REDUCES LIVER FIBROSIS IN A DOSE-DEPENDENT MANNER IN BDL RATS

Marked hepatic fibrosis was observed in BDL rats by days 17-18 (Fig. 1A). There was a dose-dependent reduction in CPA with low-dose (17.6% $\pm$ 2.5%, $P =$ 0.12) and high-dose (12.7% $\pm$ 1.9%, $P \leq$ 0.01) EDP-305 treatment compared to BDL control (22.9% $\pm$ 2.2%) (Fig. 1B). These findings were corroborated by hydroxyproline analysis (Fig. 1C); high-dose EDP-305 treatment reduced hydroxyproline levels in whole liver tissue samples compared to BDL control (control, 751 $\pm$ 46 μg/g versus EDP-305 30 mg/kg, 562 $\pm$ 56 μg/g; $P \leq$ 0.05). EDP-305 30 mg/kg also reduced messenger RNA (mRNA) relative quantification (RQ) for both Col1a1 (control, 1.1 $\pm$ 0.2 versus EDP-305 30 mg/kg, 0.58 $\pm$ 0.14; $P \leq$ 0.05) and actin, alpha 2, smooth muscle, aorta (Acta2) (control, 1.0 $\pm$ 0.14 versus EDP-305 30 mg/kg, 0.6 $\pm$ 0.16; $P \leq$ 0.05) (Fig. 1D,E). Taken together, these findings suggest a protective antifibrotic effect by EDP-305.

COLLAGEN MOLECULAR MRI CONFIRMS A REDUCTION IN LIVER FIBROSIS WITH EDP-305 TREATMENT IN THE BDL MODEL

MR images were acquired before and after contrast injection with the type 1 collagen-targeted molecular probe EP-3533, where liver relaxation rate (R1) change is directly proportional to probe uptake and to the degree of tissue fibrosis (Fig. 1F).[21] Consistent with the histologic, biochemical, and gene expression assessments of hepatic fibrosis, EDP-305 30 mg/kg treatment was associated with a reduction in liver ΔR1 compared to BDL control (ΔR1 = 0.75 $\pm$ 0.07 second^{-1} versus 1.04 $\pm$ 0.10 second^{-1}, respectively; $P \leq$ 0.05) (Fig. 1G).

EDP-305 REDUCES LIVER FIBROSIS IN A DOSE-DEPENDENT MANNER IN CDAHFD MICE

Mice administered the CDAHFD were smaller compared to mice fed regular chow ($P \leq$ 0.01), and had less gonadal and visceral fat (Supporting Fig.
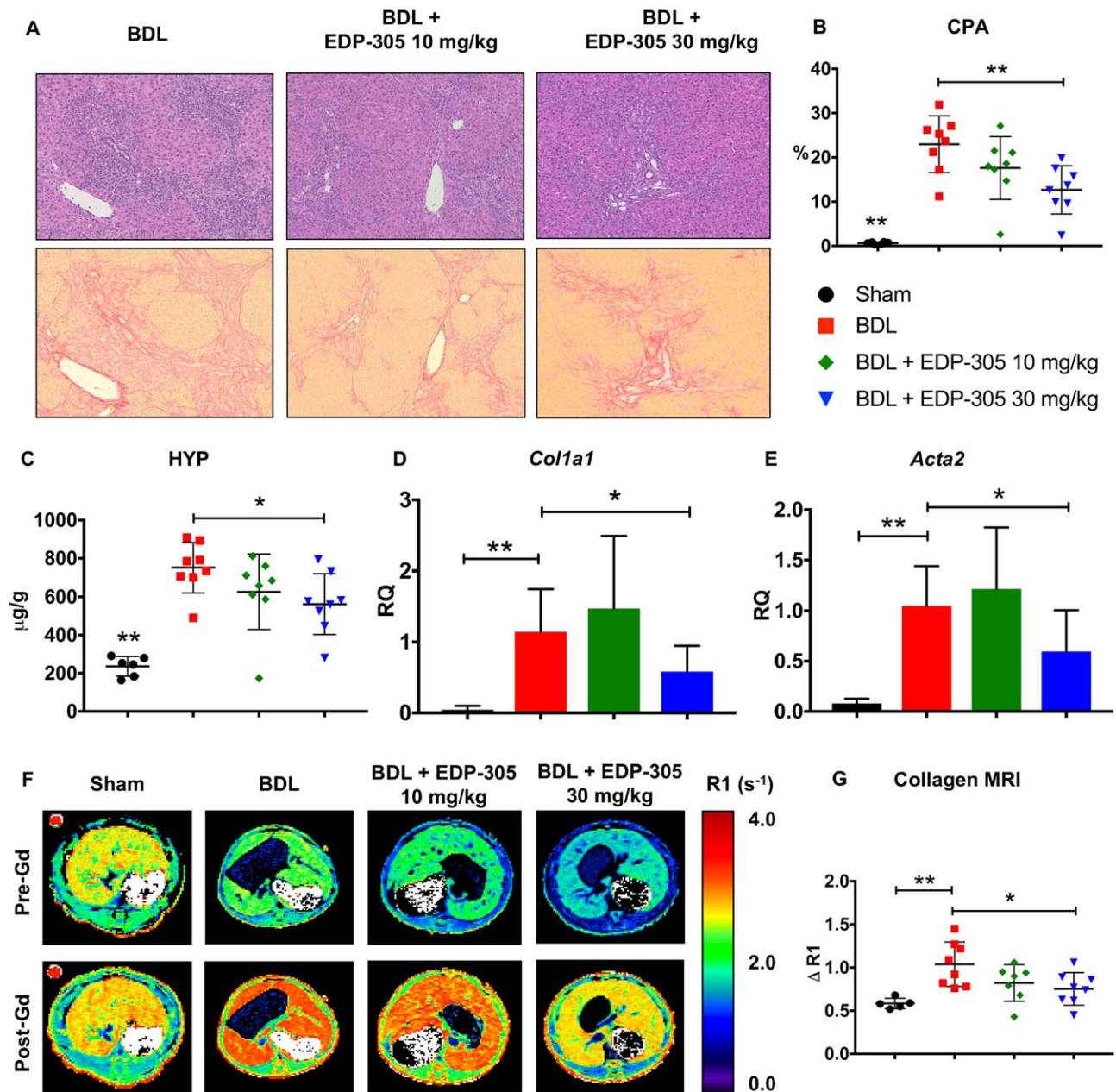
FIG. 1. EDP-305 reduces liver fibrosis in a dose-dependent manner in BDL rats. (A) Hematoxylin and eosin- (top row) and picrosirius red- (bottom row) stained liver tissue. Marked hepatic fibrosis and inflammatory infiltrates were observed in BDL-treated rats by days 17-18. Whole slide scanned sections shown at 10X magnification. (B) Percentage of collagen proportional area. (C) Hydroxyproline quantitation ($\mu g/g$) from whole liver tissue. (D) Whole liver mRNA expression of *Col1a1*. (E) Whole liver mRNA expression of *Acta2*. (F) Representative axial R1 map images of the liver for each treatment group before and after injection of the EP-3533 probe. (G) Change in relaxivity (ΔR1) in liver tissue as a surrogate measure of probe binding. All data shown as mean $\pm$ SD. *$P <$ 0.05, **$P <$ 0.01. Abbreviations: *Acta2*, actin, alpha 2, smooth muscle, aorta; HYP, hydroxyproline.

S2A). Absolute liver weight was significantly greater ($P \leq 0.01$) with high-dose EDP-305 treatment (2.44 $\pm$ 0.06 g) compared to both CDAHFD untreated control (1.81 $\pm$ 0.09 g) and regular chow (1.41 $\pm$ 0.02 g). Spleen weights were greater ($P \leq 0.05$) in mice fed the CDAHFD compared to regular chow (0.09 $\pm$ 0.003 g versus 0.07 $\pm$ 0.007 g). Compared to mice fed regular chow, mice fed the CDAHFD had elevated

aminotransferases including alanine aminotransferase (56 ± 8 U/L versus 193 ± 9 U/L; $P \leq 0.01$) and alkaline phosphatase (50 ± 2 U/L versus 100 ± 4 U/L; $P \leq 0.01$) (Supporting Fig. S2B). EDP-305 30 mg/kg (38 ± 4 mg/dL) was associated with reduced ($P \leq 0.01$) serum triglycerides compared to regular chow (80 ± 9 mg/dL).

CDAHFD mice exhibited hepatic bridging fibrosis by 12 weeks (Fig. 2A). Collagen deposition, as measured by CPA, was reduced with EDP-305 30 mg/kg (14.8% ± 1.4%, $P \leq 0.05$) compared to CDAHFD untreated control (20.4% ± 1.9%) (Fig. 2B). Similar findings were observed with hydroxyproline analysis; EDP-305 treatment significantly reduced hydroxyproline in a dose-dependent manner (EDP-305 30 mg/kg, 612 ± 39 μg/g; $P \leq 0.01$) compared to CDAHFD untreated control (835 ± 29 μg/g) (Fig. 2C). *Col1a1* mRNA expression from whole liver was reduced with high-dose EDP-305 treatment compared to CDAHFD untreated control (RQ = 1.13 ± 0.12 versus 0.67 ± 0.12; $P \leq 0.05$) (Fig. 2D), but no difference in *Acta2* mRNA expression was observed among treatment groups (Fig. 2E).

MOLECULAR MRI OF OXIDIZED COLLAGEN CONFIRMS A DOSE-DEPENDENT REDUCTION IN LIVER FIBROSIS WITH EDP-305 TREATMENT IN CDAHFD MICE

Lysyl oxidase (LOX) is a quinone-containing copper-dependent enzyme that oxidizes the terminal amino group of lysine to a reactive aldehyde (allysine), an essential step in collagen cross-linking. LOX activity has been shown to be increased in liver fibrosis and contributes to disease pathogenesis.[32] Gd-Hyd binds to allysine residues present in oxidized collagen, providing a noninvasive marker of fibrogenesis (Supporting Fig. S3). Representative MR images with a Gd-Hyd probe are shown for each treatment group (Fig. 3A). There was a dose-dependent reduction in MR liver signal intensity in the EDP-305 treatment groups compared to the CDAHFD untreated control, which reached significance at the 30-mg/kg dose (% ΔSNR = 10.7 ± 1.0 versus 6.0 ± 0.8; $P \leq 0.05$) (Fig. 3B). Fibrogenesis imaging with Gd-Hyd significantly correlated with histologic collagen quantitation (R^2 = 0.37, $P \leq 0.01$) (Fig. 3C).

We also measured expression of *Lox* and *Loxl1-4*, which are genes responsible for lysyl oxidase enzymatic activity. Expression patterns mirrored our findings with Gd-Hyd imaging, with EDP-305 treatment resulting in a dose-dependent reduction in mRNA expression of lysyl oxidase genes (Fig. 3D).

Taken together, Gd-Hyd imaging of oxidized collagen closely correlated with histologic, biochemical, and mRNA markers of disease and serves as a novel, noninvasive marker for measuring hepatic fibrogenesis.

EDP-305 DELAYS PROGRESSION OF HEPATIC INJURY IN THE CDAHFD MODEL OF NASH

To investigate the effect of EDP-305 on steatosis more thoroughly, liver fat was measured by MRI and compared among cohorts (Fig. 4A,C). Liver fat fraction was increased ($P \leq 0.05$) in both EDP-305 treatment groups (10 mg/kg, 32.5% ± 1.9%; 30 mg/kg, 32.2% ± 1.7%) compared to CDAHFD untreated control (23.6% ± 1.7%). We also assessed lipid vacuolization (percentage), which was also morphometrically quantitated from hematoxylin and eosin-stained slides of liver samples (Fig. 4B). Compared to mice fed CDAHFD (33.0% ± 1.3%), both EDP-305 treatment groups were associated with significantly increased ($P \leq 0.05$) lipid vacuolization (10 mg/kg, 38.7% ± 0.9%; 30 mg/kg, 39.9% ± 1.2%) (Fig. 4D). There was a strong correlation between the MR estimation of liver fat and the histologic morphometric fat quantification (R^2 = 0.93) (Fig. 4E). These findings indicate that noninvasive assessment of steatosis can be performed during the same MR scans used to measure fibrosis and fibrogenesis to more accurately assess hepatic disease. Finally, pathologic grading of steatosis was performed, although no difference among CDAHFD treatment groups was found (Fig. 4F). Steatosis grading by current criteria appears less sensitive than MR and morphometric quantification techniques.

To contextualize our findings, we performed a natural history experiment in which mice administered CDAHFD were analyzed at 2, 6, 10, and 14 weeks (Fig. 5A). We observed a progressive increase in fibrosis over time by CPA (Fig. 5B). There was diffuse bridging fibrosis with nodularity by 14 weeks, consistent with cirrhosis. Fibrogenic gene expression correlated well with histologic findings. *Col1a1* mRNA rapidly increased by approximately 10-fold within 2 weeks of starting the diet (RQ = 1.0 ± 0.4 versus 10.8 ± 7.9; $P \leq 0.05$) and remained stably elevated until week 14 when it increased to approximately 100-fold
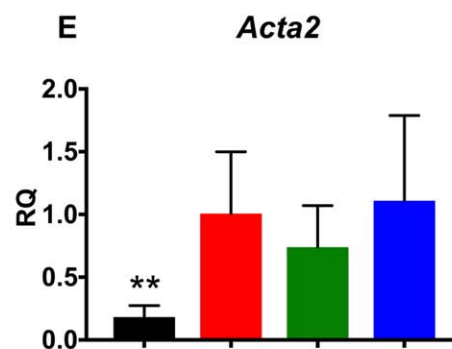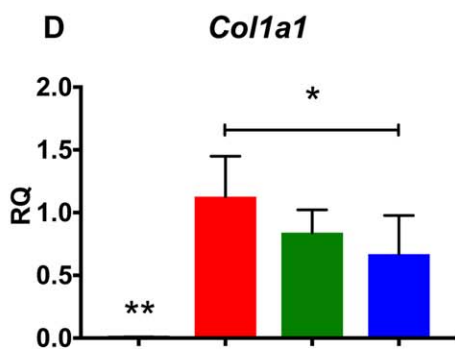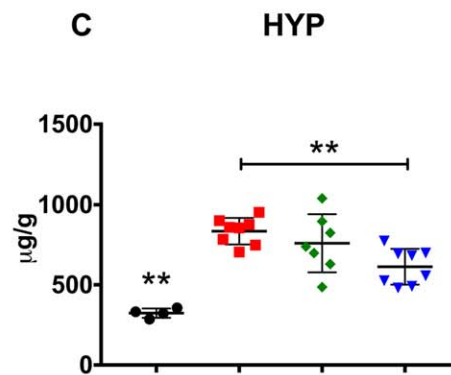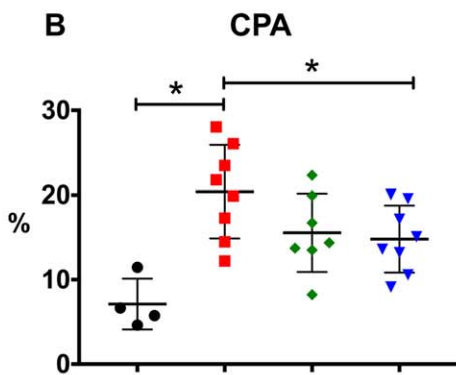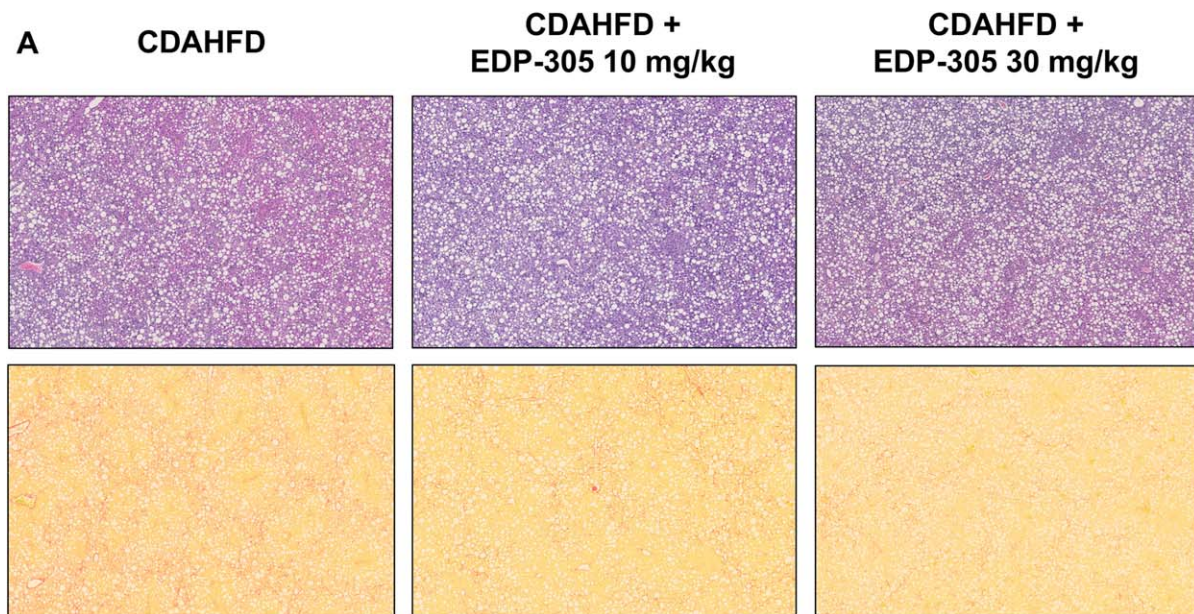
FIG. 2. EDP-305 reduces liver fibrosis in a dose-dependent manner in CDAHFD mice. (A) Hematoxylin and eosin- (top row) and picrosirius red- (bottom row) stained liver tissue. Significant steatosis and inflammation is observed in all CDAHFD treatment groups. Whole slide scanned sections shown at 2.5X magnification. (B) Percentage of collagen proportional area. (C) Hydroxyproline quantitation (μg/g) from whole liver tissue. (D) Whole liver *Col1a1* mRNA expression. (E) Whole liver alpha smooth muscle actin mRNA expression. All data shown as mean $\pm$ SD. *$P < 0.05$, **$P < 0.01$. Abbreviations: *Acta2*, actin, alpha 2, smooth muscle, aorta; HYP, hydroxyproline.
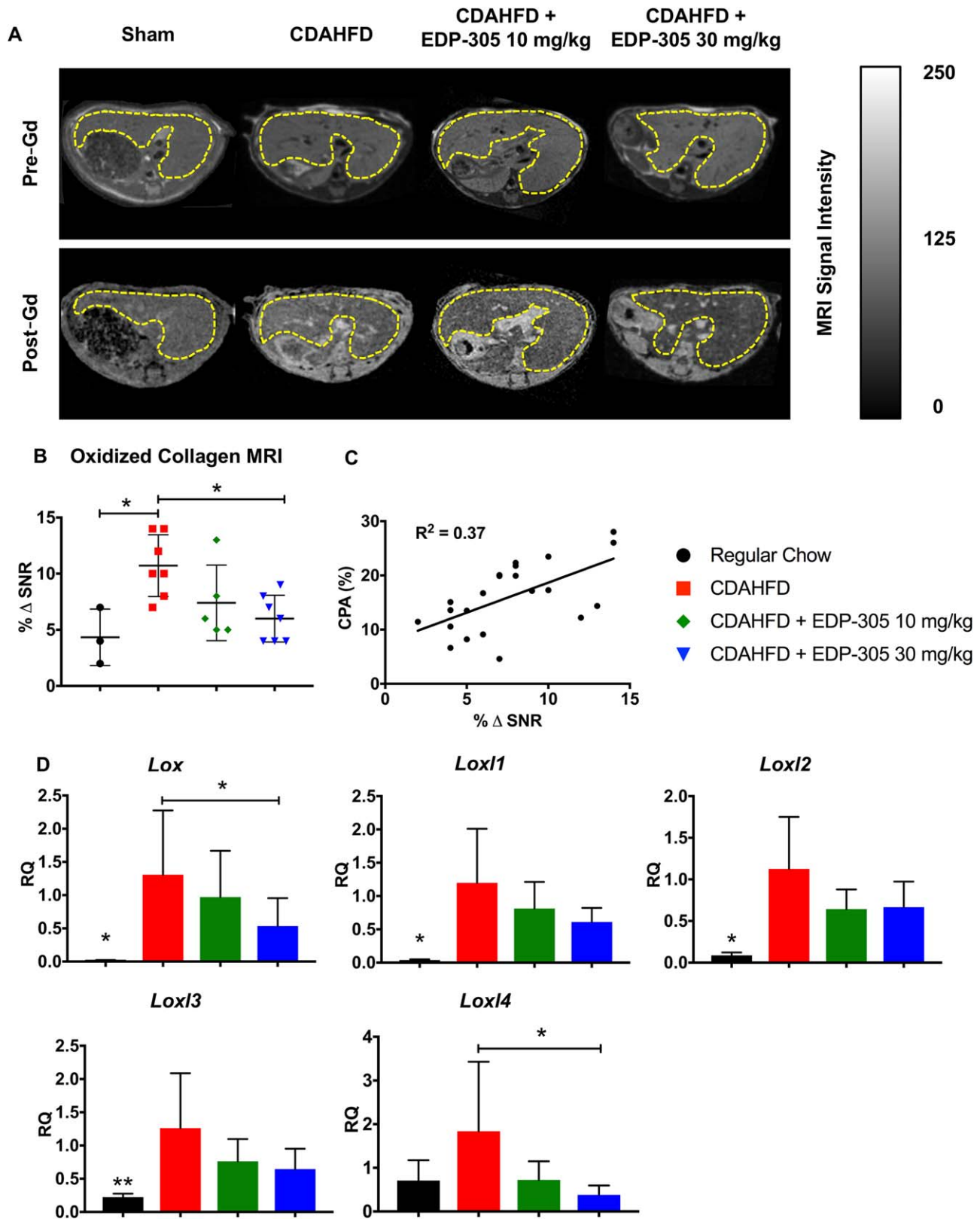
FIG. 3. Molecular imaging of oxidized collagen reveals a decrease in liver fibrogenesis with EDP-305 therapy. (A) Representative T1 MR axial images of the liver for each treatment group using the Gd-Hyd probe. Liver tissue is outlined in yellow. (B) Percentage change in liver signal to noise ratio (% ΔSNR) 35 minutes after probe injection. (C) Correlation between CPA and % ΔSNR. (D) Lysyl oxidase and lysyl oxidase paralog mRNA expression from whole liver tissue samples. All data shown as mean ± SD. *$P < 0.05$, **$P < 0.01$.
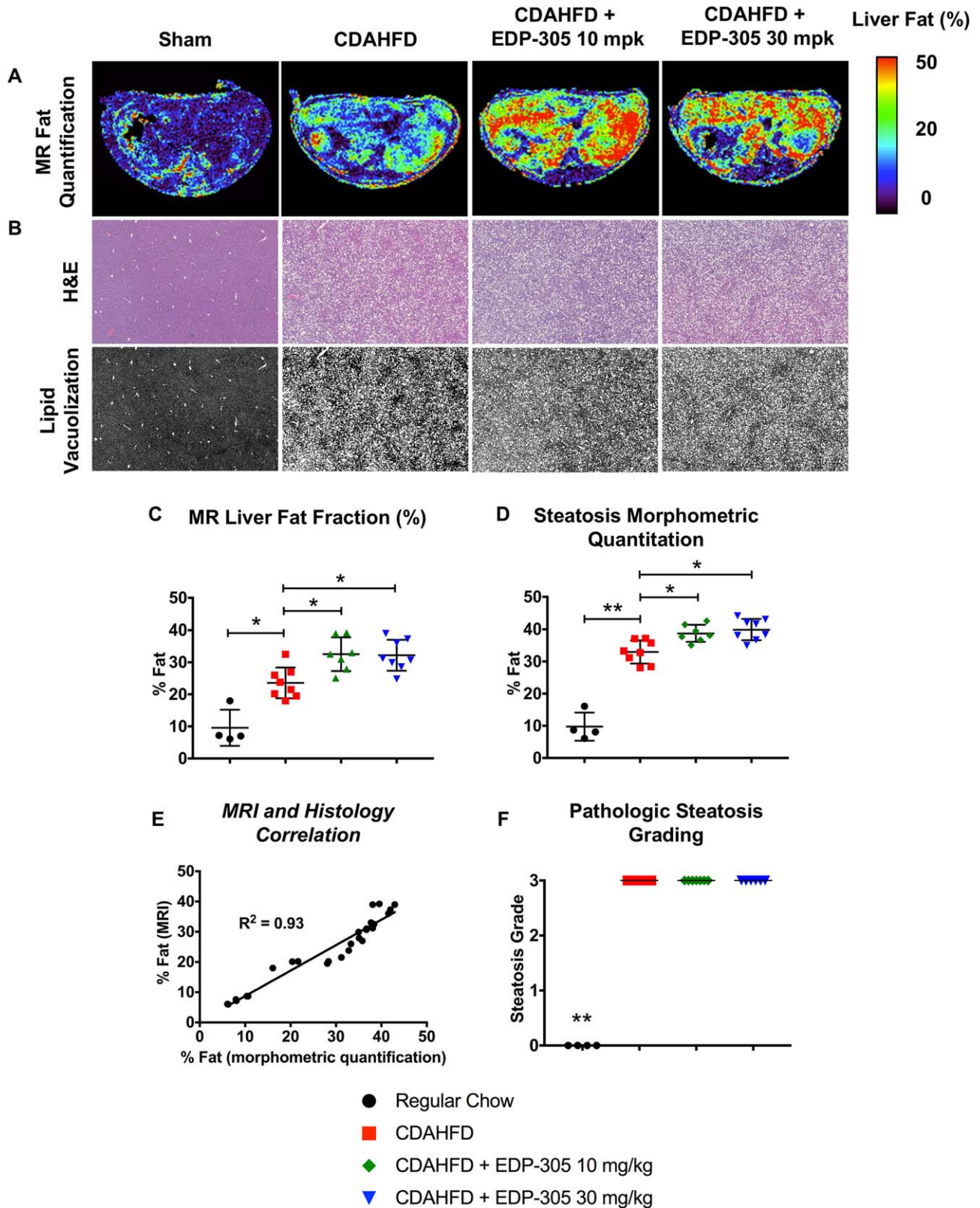
FIG. 4. Changes in hepatic steatosis with FXR therapy in CDAHFD mice. (A) Representative liver fat fraction axial images measured by the Dixon MR sequence from each treatment group. (B) Representative H&E images of liver tissue from each experimental group. Slide images were converted to black and white scaling to highlight differences in steatosis. Whole slide scanned sections are shown at 2.5X magnification. (C) Fat fraction (%) in liver tissue using the Dixon MR protocol. (D) Histologic morphometric quantitation of hepatic steatosis. (E) Dixon MR findings highly correlate with histologic morphometric fat quantification. (F) Pathologic grading of steatosis. All data shown as mean ± SD. *$P < 0.05$, **$P < 0.01$. Abbreviation: H&E, hematoxylin and eosin.
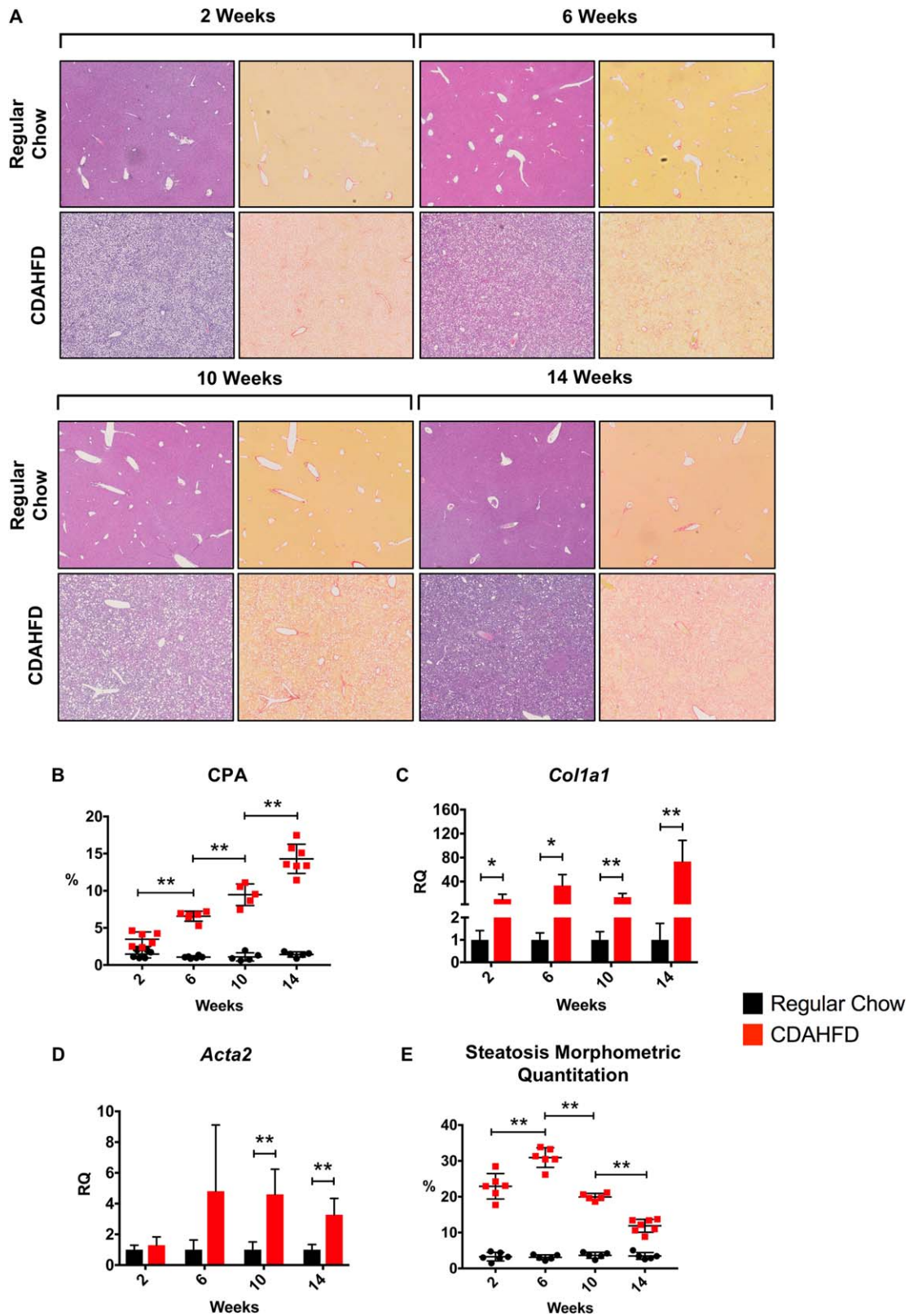
FIG. 5. Natural history of the CDAHFD model: early steatosis followed by progressive fibrosis and cirrhosis. (A) CDAHFD and regular chow mice were analyzed at 2, 6, 10, and 14 weeks for fibrosis and steatosis. Hematoxylin and eosin- (left) and picrosirius red- (right) stained liver tissue for each time point. Whole scanned slide sections are shown at 3.5X magnification. (B) There was a progressive increase in fibrosis throughout the duration of the study by CPA measurement. (C) qPCR expression of *Col1a1* mRNA revealed a 10-fold induction at 2 weeks on CDAHFD and 100-fold by 14 weeks. (D) qPCR of *Acta2* mRNA expression significantly increased by 6 weeks and remained stably elevated. (E) Steatosis increased by 2 weeks, peaked at approximately 6 weeks, after which there was a progressive decline. All data shown as mean ± SD. *$P < 0.05$, **$P < 0.01$. Abbreviations: *Acta2*, actin, alpha 2, smooth muscle, aorta; qPCR, quantitative polymerase chain reaction.

greater than regular chow-fed mice (Fig. 5C). *Acta2* expression did not significantly increase until week 10 on the diet (RQ = 1.0 ± 0.5 versus 4.6 ± 1.6; $P \leq$ 0.01), and remained stably elevated for the duration of the experiment (Fig. 5D).

Regarding steatosis, there was an initial increase starting at 2 weeks that peaked at approximately 6 weeks of diet, at which time there was also marked inflammation with fibrous expansion of portal tracts and occasional bridging septa. Beyond week 6, there was a progressive decline in hepatic lipid content as liver injury and fibrosis worsened (Fig. 5E). By week 14, livers were cirrhotic with minimal steatosis.

The CDAHFD model produces rapid and severe lipotoxic hepatic injury by preventing very low-density lipoprotein production and hepatocyte lipid transport.[25] As evidenced by the natural history experiment, the capacity to store lipid is a marker of retained hepatocyte function that dissipates shortly after 6 weeks of diet. A similar pattern of progressive fibrosis and decreasing steatosis is observed in the human form of NASH: fatty liver progresses to steatohepatiitis, followed by worsening fibrosis over years that culminates in cirrhosis, at which point minimal hepatic fat is observed.

In this context, we compared histologic samples from the CDAHFD natural history experiment with animals treated with FXR agonists. CDAHFD untreated control animals at 12 weeks appeared similar to the 10-week time point, as expected, with marked portal-to-portal and portal-to-central bridging fibrosis, significant inflammation, and reduced steatosis. In contrast, the histology from both EDP-305 treatment groups appeared more similar to the 6-week time point, with less fibrosis and increased steatosis. Given that these mice were on the diet for 6 weeks prior to an additional 6 weeks of the diet with the drug, this observation suggests that EDP-305 halted disease progression and retained hepatocyte lipid storage function.

EDP-305 ACTIVATES FXR SIGNALING IN HEPATOCYTES BUT NOT STELLATE CELLS

The FXR pathway is active in multiple tissue types, including liver, ileum, fat, and muscle. It is not well established in which organs the pathway must be stimulated to observe an antifibrotic effect in the liver, although endocrine signaling from the terminal ileum and direct hepatic stimulation are suspected to be most

relevant. We thus examined FXR pathway expression in liver and ileum of mice treated with EDP-305. Mice that were imaged received their last dose of drug 24 hours prior to sacrifice when the drug had already cleared. We therefore performed an additional experiment in which C57BL/6 mice aged 8-10 weeks were treated with EDP-305 by oral gavage for 5 days. FXR target gene expression in liver and intestine were determined by real-time polymerase chain reaction 4 hours after the last dose. EDP-305 was observed to have direct effects on the terminal ileum and liver. In the small intestine, EDP-305 treatment resulted in a dose-dependent induction in fibroblast growth factor 15 (*Fgf15*) mRNA (Supporting Fig. S4A). In the liver, EDP-305 resulted in a dose-dependent induction in small heterodimer partner (*Shp*) mRNA and concomitant reduction in cholesterol 7-alpha-monooxygenase (*Cyp7a1*) expression (Supporting Fig. S4B).

Given the observed direct hepatic effect, we next explored baseline FXR-related gene expression in untreated primary human hepatocytes, primary human stellate cells, and multiple immortalized human, mouse, and rat HSC lines *in vitro* to better understand FXR signaling in the liver (Fig. 6A). Primary human hepatocytes expressed mRNA for *FXR* and its downstream targets *SHP* and *FGF19*, as well as *FGFR4*, the transmembrane receptor for FGF19. We did not observe baseline expression of *FXR* or its downstream targets in isolated primary human HSCs, although we did observe low-level expression of *FGFR4* mRNA. The immortalized human stellate cell line LX2 expressed low levels of mRNA for *FXR*, *SHP*, and *FGFR4* but not *FGF19*, whereas TWNT4, another immortalized human stellate line, expressed no mRNA for these genes. B8 immortalized rat stellate cells and immortalized mouse stellate cells both expressed low levels of *Fxr* and *Fgfr4* mRNA.

Relative to hepatocytes and mouse whole liver samples, all stellate cell lines had insignificant expression of FXR-related genes (Fig. 6B). These findings were corroborated by FXR and FGFR4 protein expression on western blot (Fig. 6C). Both proteins were highly expressed in whole mouse liver and primary human hepatocytes, suggesting possible biologic relevance for both direct hepatic FXR stimulation and endocrine FGF15/19 signaling from the terminal ileum by portal circulation. In contrast, primary human HSCs and all stellate lines had significantly lower expression of FGFR4, and only faint FXR expression was observed in B8 rat stellate cells. Treatment of serum-starved human hepatocytes in culture with EDP-305 at 10
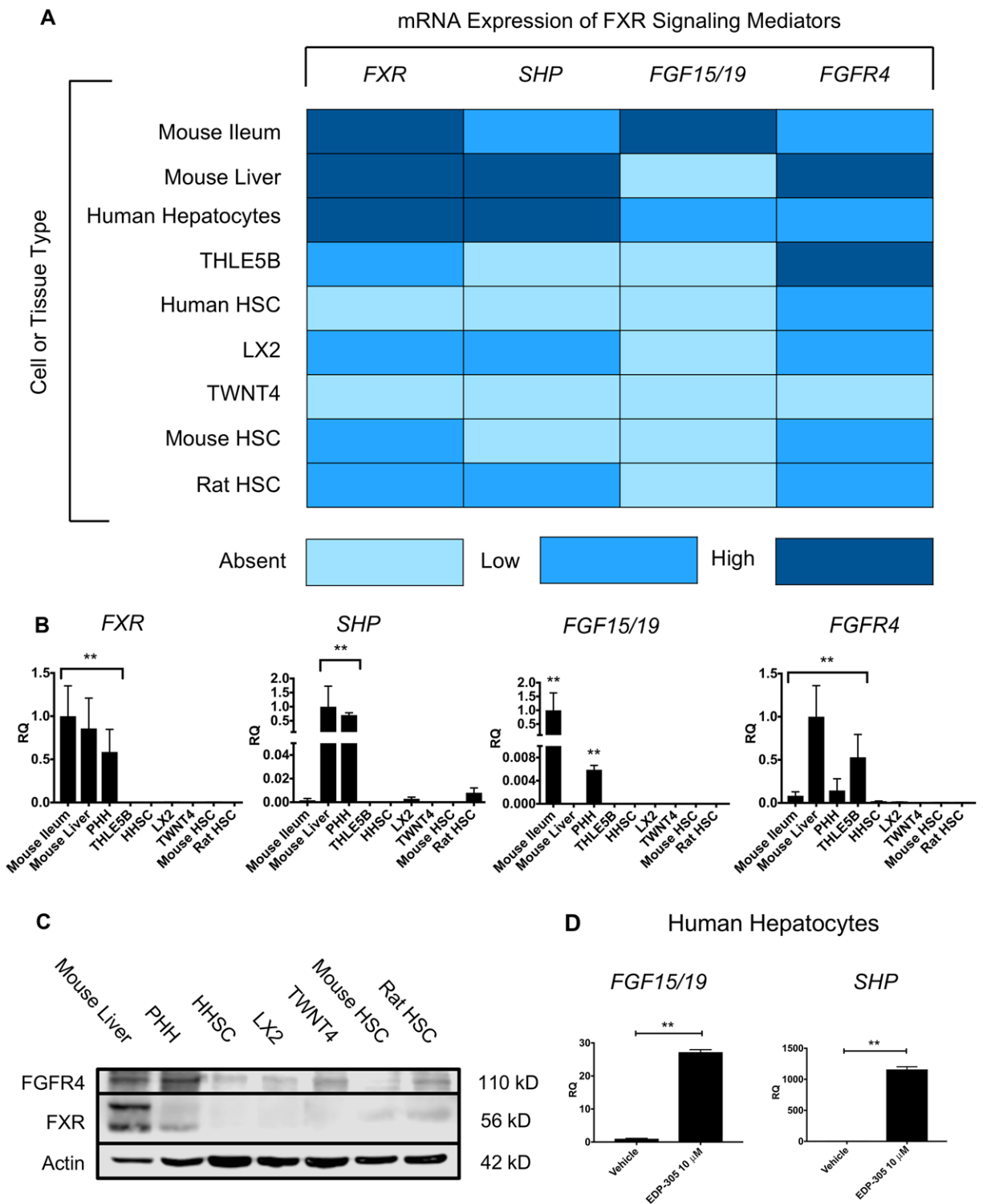
FIG. 6. EDP-305 directly activates liver hepatoctyes but not stellate cells. (A) Liver, ileum, hepatocyte, and stellate cell mRNA for *FXR*, *SHP*, *FGF19*, and *FGFR4*. Light blue represents no expression, blue represents low expression, and dark blue represents high expression. (B) Stellate cell lines had insignificant mRNA expression of FXR-related genes relative to hepatocytes and mouse whole liver tissue. (C) FXR and FGFR4 protein expression with western blot. (D) EDP-305-induced mRNA expression of *FGF19* and *SHP* in primary human hepatocytes. All data shown as mean ± SD. *$P < 0.05$, **$P < 0.01$. Abbreviations: PHH, primary human hepatocytes; HHSC, human hepatic stellate cells.

μM for 72 hours induced mRNA expression of *SHP* and *FGF19* (Fig. 6D). However, of the stellate lines that expressed *FXR* mRNA, treatment *in vitro* with EDP-305 elicited no induction of downstream targets *SHP* or *FGF15/19* (data not shown). These findings indicate that FXR is expressed at higher levels in hepatocytes compared to stellate cells, and evidence of FXR pathway activation was only present in hepatocytes.

Similar findings have been reported. Fickert et al.[33] evaluated FXR expression in mice and humans, and similar to our current findings, they observed low/nonexistent levels of FXR in HSCs and myofibroblasts but higher levels in hepatocytes. However, other studies have also reported FXR protein expression in isolated primary rat HSCs and the immortalized line HSC-T6.[34] Taken together, these findings suggest that hepatic FXR agonism, at least in mice and humans, is unlikely to directly affect stellate cells.

Discussion

EDP-305 is a steroidal noncarboxylic acid FXR agonist that is currently in clinical trials for NASH and PBC.[35-38] We observed significant reductions in liver fibrosis with EDP-305 in two rodent models of hepatic injury, corroborated by multiple methodologies, including picrosirius red collagen staining, hydroxyproline biochemical quantification, gene expression analyses, and noninvasive molecular imaging. This study represents the first published data for EDP-305 showing a potent and consistent antifibrotic effect *in vivo* in animal models of cholestatic and non-alcoholic fatty liver injury.

We chose hepatic fibrosis as the primary endpoint of our study because it is a critical pathogenic component of chronic liver injury and cirrhosis. Fibrosis secondary to either biliary or direct hepatocyte damage is driven primarily by myofibroblastic activation of HSCs, which deposit dense networks of extracellular matrix, including proteoglycans and collagens.[39,40] It is thought that fibrosis is a natural wound healing response that goes awry in the setting of persistent tissue injury. As fibrosis becomes more severe, it may have multiple negative effects in the liver, including obstruction of biliary canaliculi, venous congestion, and support of a proinflammatory milieu through HSC-mediated secretion of inflammatory signaling molecules.[41] These processes may exacerbate the effects from ongoing hepatic insults, contributing to progressive liver failure. Therefore, mitigation of fibrosis in the setting of chronic liver disease has become a therapeutic goal in and of itself.

Our focus on liver fibrosis influenced our selection of rodent models for hepatic injury. Choosing the appropriate animal model for studying cholestatic and fatty liver injury can be a challenging endeavor as currently available models recapitulate only certain aspects of human disease. NASH is typically observed in patients with obesity and associates with metabolic syndromes, including hypertension and insulin resistance. However, simultaneously establishing metabolic dysregulation and steatohepatitis that leads to progressive liver failure has proven difficult, and currently available models typically accentuate either the metabolic or the hepatotoxic components.[42] In this regard, the Western diet, consisting of high fat and high fructose, most accurately captures the dietary habits of humans, and indeed obesity and insulin resistance are observed.[43] However, this model requires multiple months to develop evidence of hepatic fibrosis, which remains mild to moderate in severity throughout the course of disease. The CDAHFD lacks the metabolic derangements observed in NASH, but the choline deficiency provides a severe lipotoxic hepatic injury and robust fibrotic response.[25] We therefore chose to use a choline-deficiency model despite the acknowledged metabolic limitations. Other hepatocyte injury models, including amylin liver NASH and genetically engineered mutant strains, induce only modest inflammation and fibrosis compared to choline deficiency.

Similarly, PBC is thought to be an autoimmune process targeting epithelial cholangiocytes, which results in biliary injury, cholestasis, and eventually cirrhosis and hepatic failure.[44] Multiple cholestatic rodent models exist, and some recapitulate certain immunologic features of PBC. However, these models are associated with only mild hepatic fibrosis. Conversely, the BDL model bares no immunologic resemblance to PBC, although the profound cholestatic injury in this model induces a robust fibrotic response that more accurately mirrors severe stages of human cholestatic disease.

Based on our *in vitro* data, the antifibrotic effects of FXR agonism observed with EDP-305 are likely mediated by direct hepatocyte signaling with secondary effects on stellate cells. The minimal expression of FXR pathway components that we observed in mouse and human HSCs did not appear biologically relevant based on gene and protein expression analyses. This was supported by a lack of induction of putative FXR target genes with agonist treatment *in vitro*.

Interestingly, we did observe expression of FXR in rat HSCs, albeit at a low level. Fiorucci et al.[34] showed that FXR agonism in rat HSCs was associated with an induction of SHP with concomitant reductions in *Col1a1*, *Acta2*, and transforming growth factor-beta. Taken together, these findings indicate that FXR signaling in HSCs may be species dependent.

Finally, molecular MR imaging of type 1 collagen (EP-3533) and oxidized collagen (Gd-Hyd) in the BDL and CDAHFD models, respectively, are sensitive measures for detecting changes in fibrosis in response to treatment and were consistent with other biochemical and gene expression analyses. The imaging methods used in this study thus have potential for future clinical application.[19,21] Other modalities for imaging hepatic fibrosis are being trialed. Fibrosis results in an overproduction of matrix proteins that cause tissue stiffness, which can be measured by elastography.[45] Ultrasound and MR-based elastography are two promising modalities that are currently used in the clinical setting.[46,47] Our group previously compared MR elastography and EP-3533 in a diethylnitrosamine-induced model of rat fibrosis and found that collagen imaging was more sensitive at earlier stages of fibrosis and may provide value in this regard.[22] Further comparison between MR elastography and collagen molecular imaging is thus needed.

In conclusion, EDP-305 demonstrated its ability to reduce liver injury and hepatic fibrosis progression. These findings indicate that EDP-305 may have clinical relevance for the treatment of human conditions characterized by biliary or hepatic fibrosis.

REFERENCES

1) Fang S, Suh JM, Reilly SM, Yu E, Osborn O, Lackey D, et al. Intestinal FXR agonism promotes adipose tissue browning and reduces obesity and insulin resistance. Nat Med 2015;21:159-165.

2) Kim KH, Choi S, Zhou Y, Kim EY, Lee JM, Saha PK, et al. Hepatic FXR/SHP axis modulates systemic glucose and fatty acid homeostasis in aged mice. Hepatology 2017;66:498-509.

3) Sinal CJ, Tohkin M, Miyata M, Ward JM, Lambert G, Gonzalez FJ. Targeted disruption of the nuclear receptor FXR/BAR impairs bile acid and lipid homeostasis. Cell 2000;102:731-744.

4) Pollheimer MJ, Halilbasic E, Fickert P, Trauner M. Pathogenesis of primary sclerosing cholangitis. Best Pract Res Clin Gastroenterol 2011;25:727-739.

5) Thompson MD, Moghe A, Cornuet P, Marino R, Tian J, Wang P, et al. beta-Catenin regulation of farnesoid X receptor signaling and bile acid metabolism during murine cholestasis. Hepatology 2018;67:955-971.

6) Fischer S, Beuers U, Spengler U, Zwiebel FM, Koebe HG. Hepatic levels of bile acids in end-stage chronic cholestatic liver disease. Clin Chim Acta 1996;251:173-186.

7) Ibrahim SH, Hirsova P, Gores GJ. Non-alcoholic steatohepatitis pathogenesis: sublethal hepatocyte injury as a driver of liver inflammation. Gut 2018;67:963-972.

8) Xu J, Li Y, Chen WD, Xu Y, Yin L, Ge X, et al. Hepatic carboxylesterase 1 is essential for both normal and farnesoid X receptor-controlled lipid homeostasis. Hepatology 2014;59:1761-1771.

9) Ong JP, Younossi ZM. Epidemiology and natural history of NAFLD and NASH. Clin Liver Dis 2007;11:1-16.

10) Sayiner M, Koenig A, Henry L, Younossi ZM. Epidemiology of nonalcoholic fatty liver disease and nonalcoholic steatohepatitis in the United States and the rest of the world. Clin Liver Dis 2016;20:205-214.

11) Poonawala A, Nair SP, Thuluvath PJ. Prevalence of obesity and diabetes in patients with cryptogenic cirrhosis: a case-control study. Hepatology 2000;32:689-692.

12) Diehl AM. Nonalcoholic steatosis and steatohepatitis IV. Nonalcoholic fatty liver disease abnormalities in macrophage function and cytokines. Am J Physiol Gastrointest Liver Physiol 2002;282:G1-G5.

13) Lindor KD, Gershwin ME, Poupon R, Kaplan M, Bergasa NV, Heathcote EJ, et al.; American Association for Study of Liver Diseases. Primary biliary cirrhosis. Hepatology 2009;50:291-308.

14) Carey EJ, Ali AH, Lindor KD. Primary biliary cirrhosis. Lancet 2015;386:1565-1575. Erratum in: Lancet 2015;386:1536.

15) U.S. Food & Drug Administration. FDA Drug Safety Communication: FDA warns about serious liver injury with Ocaliva (obeticholic acid) for rare chronic liver disease. https://www.fda.gov/Drugs/DrugSafety/ucm576656.htm. Published September 21, 2017. Accessed September 2017.

16) Motola DL, Caravan P, Chung RT, Fuchs BC. Noninvasive biomarkers of liver fibrosis: clinical applications and future directions. Curr Pathobiol Rep 2014;2:245-256.

17) Terjung B, Lemnitzer I, Dumoulin FL, Effenberger W, Brackmann HH, Sauerbruch T, et al. Bleeding complications after percutaneous liver biopsy. An analysis of risk factors. Digestion 2003;67:138-145.

18) **Chen HH, Waghorn PA**, Wei L, Tapias LF, Schu Hle DT, Rotile NJ, et al. Molecular imaging of oxidized collagen quantifies pulmonary and hepatic fibrogenesis. JCI Insight 2017;2.

19) **Fuchs BC, Wang H**, Yang Y, Wei L, Polasek M, Schühle DT, et al. Molecular MRI of collagen to diagnose and stage liver fibrosis. J Hepatol 2013;59:992-998.

20) **Farrar CT, DePeralta DK**, Day H, Rietz TA, Wei L, Lauwers GY, et al. 3D molecular MR imaging of liver fibrosis and response to rapamycin therapy in a bile duct ligation rat model. J Hepatol 2015;63:689-696.

21) **Polasek M, Fuchs BC**, Uppal R, Schühle DT, Alford JK, Loving GS, et al. Molecular MR imaging of liver fibrosis: a feasibility study using rat and mouse models. J Hepatol 2012;57:549-555.

22) Zhu B, Wei L, Rotile N, Day H, Rietz T, Farrar CT, et al. Combined magnetic resonance elastography and collagen molecular magnetic resonance imaging accurately stage liver fibrosis in a rat model. Hepatology 2017;65:1015-1025.

23) Pfeifer AM, Cole KE, Smoot DT, Weston A, Groopman JD, Shields PG, et al. Simian virus 40 large tumor antigen-immortalized normal human liver epithelial cells express

hepatocyte characteristics and metabolize chemical carcinogens. Proc Natl Acad Sci U S A 1993;90:5123-5127.

24) DePeralta DK, Wei L, Ghoshal S, Schmidt B, Lauwers GY, Lanuti M, et al. Metformin prevents hepatocellular carcinoma development by suppressing hepatic progenitor cell activation in a rat model of cirrhosis. Cancer 2016;122:1216-1227.

25) Matsumoto M, Hada N, Sakamaki Y, Uno A, Shiga T, Tanaka C, et al. An improved mouse model that rapidly develops fibrosis in non-alcoholic steatohepatitis. Int J Exp Pathol 2013;94:93-103.

26) Caravan P, Das B, Dumas S, Epstein FH, Helm PA, Jacques V, et al. Collagen-targeted MRI contrast agent for molecular imaging of fibrosis. Angew Chem Int Ed Engl 2007;46:8171-8173.

27) Helm PA, Caravan P, French BA, Jacques V, Shen L, Xu Y, et al. Postinfarction myocardial scarring in mice: molecular MR imaging with use of a collagen-targeting contrast agent. Radiology 2008;247:788-796.

28) Caravan P, Yang Y, Zachariah R, Schmitt A, Mino-Kenudson M, Chen HH, et al. Molecular magnetic resonance imaging of pulmonary fibrosis in mice. Am J Respir Cell Mol Biol 2013;49:1120-1126.

29) Dixon WT. Simple proton spectroscopic imaging. Radiology 1984;153:189-194.

30) Murayama KM, Barent BL, Gruber M, Brooks A, Eliason S, Brunt EM, et al. Characterization of a novel model of pancreatic fibrosis and acinar atrophy. J Gastrointest Surg 1999;3:418-425.

31) Fuchs BC, Hoshida Y, Fujii T, Wei L, Yamada S, Lauwers GY, et al. Epidermal growth factor receptor inhibition attenuates liver fibrosis and development of hepatocellular carcinoma. Hepatology 2014;59:1577-1590.

32) Ikenaga N, Peng ZW, Vaid KA, Liu SB, Yoshida S, Sverdlov DY, et al. Selective targeting of lysyl oxidase-like 2 (LOXL2) suppresses hepatic fibrosis progression and accelerates its reversal. Gut 2017;66:1697-1708.

33) Fickert P, Fuchsbichler A, Moustafa T, Wagner M, Zollner G, Halilbasic E, et al. Farnesoid X receptor critically determines the fibrotic response in mice but is expressed to a low extent in human hepatic stellate cells and periductal myofibroblasts. Am J Pathol 2009;175:2392-2405.

34) Fiorucci S, Antonelli E, Rizzo G, Renga B, Mencarelli A, Riccardi L, et al. The nuclear receptor SHP mediates inhibition of hepatic stellate cells by FXR and protects against liver fibrosis. Gastroenterology 2004;127:1497-1512.

35) National Institutes of Health. Study of safety and efficacy of tropifexor (LJN452) in patients with non-alcoholic steatohepatitis (NASH)(FLIGHT-FXR). https://ClinicalTrials.gov/show/NCT02855164. Published August 4, 2016. Accessed February 2018.

36) National Institutes of Health. The farnesoid X receptor (FXR) ligand obeticholic acid in NASH treatment trial (FLINT) (FLINT). https://ClinicalTrials.gov/show/NCT01265498. Published December 23, 2010. Accessed February 2018.

37) National Institutes of Health. Phase 3 study of obeticholic acid in patients with primary biliary cirrhosis (POISE). https://ClinicalTrials.gov/show/NCT01473524. Published November 17, 2011. Accessed February 2018.

38) National Institutes of Health. Phase 4 study of obeticholic acid evaluating clinical outcomes in patients with primary biliary cholangitis (COBALT). https://ClinicalTrials.gov/show/NCT02308111. Published December 4, 2014. Accessed February 2018.

39) Schuppan D, Surabattula R, Wang XY. Determinants of fibrosis progression and regression in NASH. J Hepatol 2018;68:238-250.

40) Hirschfield GM, Gershwin ME. The immunobiology and pathophysiology of primary biliary cirrhosis. Annu Rev Pathol 2013;8:303-330.

41) Zhou WC, Zhang QB, Qiao L. Pathogenesis of liver cirrhosis. World J Gastroenterol 2014;20:7312-7324.

42) Haczeyni F, Yeh MM, Ioannou GN, Leclercq IA, Goldin R, Dan YY, et al. Mouse models of nonalcoholic steatohepatitis: a reflection on recent literature. J Gastroenterol Hepatol 2018; doi: 10.1111/jgh.14122.

43) Henkel J, Coleman CD, Schraplau A, Jöhrens K, Weber D, Castro JP, et al. Induction of steatohepatitis (NASH) with insulin resistance in wildtype B6 mice by a western-type diet containing soybean oil and cholesterol. Mol Med 2017;23.

44) Hargrove L, Kennedy L, Demieville J, Jones H, Meng F, DeMorrow S, et al. Bile duct ligation-induced biliary hyperplasia, hepatic injury, and fibrosis are reduced in mast cell-deficient Kit(W-sh) mice. Hepatology 2017;65:1991-2004.

45) Kawamoto M, Mizuguchi T, Katsuramaki T, Nagayama M, Oshima H, Kawasaki H, et al. Assessment of liver fibrosis by a noninvasive method of transient elastography and biochemical markers. World J Gastroenterol 2006;12:4325-4330.

46) Wang Y, Ganger DR, Levitsky J, Sternick LA, McCarthy RJ, Chen ZE, et al. Assessment of chronic hepatitis and fibrosis: comparison of MR elastography and diffusion-weighted imaging. AJR Am J Roentgenol 2011;196:553-561.

47) Cui J, Ang B, Haufe W, Hernandez C, Verna EC, Sirlin CB, et al. Comparative diagnostic accuracy of magnetic resonance elastography vs. eight clinical prediction rules for non-invasive diagnosis of advanced fibrosis in biopsy-proven non-alcoholic fatty liver disease: a prospective study. Aliment Pharmacol Ther 2015;41:1271-1280.

Author names in bold designate shared co-first authorship.

Supporting Information

Additional Supporting Information may be found at onlinelibrary.wiley.com/doi/10.1002/hep4.1193/full.